Origin of Carrier-Type Reversal in Pb−Ge−Se Glasses: A Detailed Thermal, Electrical, and Structural Study[§]

B. Vaidhyanathan,[†] S. Murugavel,[‡] S. Asokan,[‡] and K. J. Rao*[,†]

Solid State and Structural Chemistry Unit and Department of Instrumentation, Indian Institute of Science, Bangalore-560 012, India

Received: July 1, 1997; In Final Form: September 3, 1997[⊗]

A long-standing and important problem in glass science has been carrier-type reversal (CTR) in semiconducting glasses. This phenomenon is exhibited by Pb−Ge−Se glasses also. It has been addressed here by carrying out detailed electrical, thermal, and spectroscopic investigations. $Pb_xGe_{42-x}Se_{58}$ ($x = 0-20$) glasses were prepared by a two stage melt-quenching process and characterized using x-ray diffraction, high-resolution electron microscropy, and energy dispersive analysis of x-rays. Thermoelectric power and high-pressure electrical resistivity have been measured. IR, Raman, and X-ray adsorption near edge structure spectroscopies have been used for examining the glass structures as well as differential scanning calorimetry (DSC) for studying the thermal properties. A structural model based on the chemical nature of the constituents has been proposed to account for the observed properties of these glasses. Effect of Pb incorporation on local structures and qualitative consequences on the energy band structures of Ge−Se glasses has been considered. The p → n transition has been attributed to the energetic disposition of the sp^3d^2 band of Pb atoms, which is located closely above the lone pair band of selenium. This feature makes Pb unique in the context of p → n transition of chalcogenide glasses. The model can be extended successfully to account for the CTR behavior observed in Bi containing chalcogenide glasses also.

1. Introduction

Chalcogenide glasses containing S or Se or Te constitute a rich family of vitreous semiconductors. There has been an intense research activity based on these glasses[1−5] because of their technological applications. The effect of impurities on the electronic properties of amorphous chalcogenides has been the subject of serious debate ever since their discovery.[6] It has long been known that these glasses, which behave like intrinsic p-type semiconductors, are insensitive to "doping" and that this behavior is attributed to the local valence saturation of the dopant atom. Fermi level is considered to be pinned due to the equilibrium between the negatively and positively charged (D^- and D^+) dangling (D) bonds.[7,8] The concept of pinned fermi level is not consistent with the discovery of the fascinating phenomenon of p → n transition or the conduction-type reversal (CTR) observed first in bismuth germanium chalcogenide glasses.[9,10] This discovery has led to further extensive research on these materials[11−17] and to a reconsideration of the existing theories of electronic structure of chalcogenide glasses.[18] The carrier type reversal in germanium chalcogenides requires incorporation of a significant amount of Bi,[9] it is considered desirable to use the term "chemical modification" rather than "doping".[19] There is vast scope for technological exploitation of the phenomenon of p → n transition observed in chalcogenide glasses such as preparation of a new class of p−n junctions[20] based entirely on glasses since it offers several manufacturing advantages.[21] There has been an avalanche of investigations[22−25] to understand the mechanism of conduction type reversal and a number of structural and electronic models have been proposed. For example, (i) the observed "doping effect" in the Bi-containing chalcogenide glasses has been ascribed to an alteration of the equilibrium between the charged defect pairs (C_1^- and C_3^+), since bismuth can be considered as entering the glassy network as a charged impurity (unpinning of the fermi level).[9] (ii) The p → n transition has been ascribed to an inhomogeneous (percolation) transport mechanism[26,27] through the phase-separated Bi_2X_3 (X = chalcogen) type of submicroscopic clusters.[16,28] This implies 6-fold coordination for Bi which has been contradicted by experimental findings.[29] (iii) CTR is considered to be highly influenced by the polarizability of the Bi atoms while the coordination of Bi is assumed to be 3.[29] But glasses containing thallium (Tl) in place of Bi do not exhibit CTR,[30] although Tl has higher polarizability. Also, since Tl enters 4-coordinated sites, it gives rise to more C_3^+ centers, which prevents CTR. In all these models a chemically ordered network (CONM) is assumed for the glass structure in which formation of heteropolar bonds are favored over homopolar bonds. Bismuth bonding with chalcogen is treated as ionocovalent in character.[29,31,32] Efforts made toward understanding CTR in Bi−Ge−Se glasses have led to the discovery of the only other chalcogenide glasses known to exhibit CTR phenomenon, and these are the lead−germanium−selenium glasses.[33] Carrier-type reversal has been observed in two series of glass compositions, viz $Pb_{20}Ge_ySe_{80-y}$ ($y = 17-24$; CTR at $y = 21$) and $Pb_xGe_{42-x}Se_{58}$ ($x = 0-20$; CTR at $x = 10$). Lead−germanium-chalcogenide glasses are also photoconducting and exhibit ambipolar conduction.[34,35] This is in contrast to the unipolar conduction observed in arsenic based semiconducting glassy chalcogenides.[36] There are several reports on the thermal[37] and electrical[38,39] properties of the $Pb_{20}Ge_ySe_{80-y}$ glasses, although not on the $Pb_xGe_{42-x}Se_{58}$ glasses. Indeed only very little information is presently available on the structure and transport properties of these glasses.[40] In the $Pb_xGe_{42-x}Se_{58}$ system, preparation of homogeneous glasses is possible over a wide range of x values and therefore changes in the various properties and structure can be thoroughly examined as a function of composition across the p → n transition. It is also possible to examine the CTR on the basis of both charged defect pair concept and qualitative energy band structure relevant to

[§] Contribution no. 1264 from the Solid State and Structural Unit.
[†] Solid State and Structural Chemistry Unit.
[‡] Department of Instrumentation.
[⊗] Abstract published in *Advance ACS Abstracts,* October 15, 1997.

S1089-5647(97)02129-9 CCC: $14.00

these glasses. In fact one of the important aspects to be addressed in this context is the uniqueness of the role of Pb or Bi in Ge−Se glasses, the presence of which leads to CTR behavior. If the p → n transition is of purely structural origin, it may not be a necessity to associate CTR with unpinning of the fermi level. This interesting CTR behavior exhibited by lead germanium chalcogenides is examined in this paper. Electrical, thermal, and spectroscopic investigations on $Pb_xGe_{42-x}Se_{58}$ ($x = 0-20$) glasses have been performed to arrive at a consistent description of the glass structure. Effect of variation of the composition on the structure as well as energy bands has been considered. Holes which are identical with C_3^+ centers migrate through a bond switching mechanism. Electron transport is attributed to bipolarons associated with C_1^- centers which move via the sp^3d^2 band of Pb atoms. Therefore, electron transport is characterized by a barrier which is the difference in pairing energies in sp^3d^2 and sp type bands. It is shown that the dominant carrier in Pb−Ge−chalcogenide glasses, which are ambipolar conductors, changes from holes to electrons as the lead content increases.

2. Experimental Section

Bulk $Pb_xGe_{42-x}Se_{58}$ ($x = 0-20$) glasses were prepared by a two-stage melt quenching process. Calculated quantities of high purity (99.999% from Fluka) constituents (Pb, Ge, and Se) were taken together in quartz ampules which were repeatedly flushed with argon and sealed under vacuum of 10^{-5} Torr. The ampules were slowly heated in a rotary furnace and kept at 873 K for about 24 h. They were subsequently heated to 1273 K and maintained at this temperature for 36 h. During this stage ampules were kept continuously rotated to ensure homogenization of the melt. The ampules were then directly quenched in ice water + NaOH mixture. Ampules were broken open to recover shiny glass plugs of the various compositions. Either powder or pieces of glass were used for various characterization experiments. X-ray diffraction (XRD; Philips X-ray diffractometer, model: PW 1050/70) and high-resolution electron microscopy (HREM; HRTEM JEOL-200CX) were used to confirm the amorphous nature of the samples. Energy-dispersive X-ray analysis (EDAX) was performed on these glasses to confirm the chemical composition. Densities (molar volumes) were determined using Archimedean principle with xylene as a densitometric fluid. A Sartorius balance was used for the weight measurements whose accuracy is 10^{-4} g. The glass transition (T_g) and crystallization (T_c) temperatures of the glasses were determined employing a Perkin-Elmer DSC-2 scanning calorimeter. Fifty milligrams of samples were used, and a heating rate of 10 °C/min was employed in the DSC experiments. Heat capacities (C_p's) were determined using single-crystal sapphire as a standard for all glasses from room temperature to temperatures exceeding $T_g + 50$ K so as to be able to determine both glass heat capacities and the change of heat capacities (ΔC_p) at the glass transition temperatures. Direct current (dc) resistivities were measured by simple two-probe technique using thin bits of glass samples with parallel surfaces coated with Ag electrodes. Contacts were ohmic and no special care was required for the measurements. Resistivities were measured as a function of temperature and the activation barriers were determined using Arrhenius plots (log ρ vs $1000/T$). Thermoelectric powers (S) of the samples were determined using rectangular glass pieces in a sandwich geometry, on a home-built apparatus which consists of a copper sample holder, nichrome coil gradient heater, a preamplifier, and a Keithley 616 electrometer. The preamplifier is made of two stages. The first stage consists of an operational amplifier (AD-542) with a high input impedance of 10^{12} Ω. In the second stage another operational amplifier (ADOP-07) with unity gain was used. The output of the second stage was measured using the electrometer. Although measurements could be made at lower temperatures, the above setup enabled us to get highly reproducible measurements (with very little scatter) around 373 K. Hence the thermo power results presented in this work were obtained at 373 K and this temperature is well below the T_g's of the samples. Measurements were performed in Ar atmosphere in order to prevent any complication arising from ambient oxygen. The experiments were repeated with Au electrodes, and the observations were confirmed to be unaffected by the nature of the electrode. Diffuse reflectance spectra were recorded on a Perkin-Elmer UV−vis Spectrophotometer, and the variation of diffuse reflectance peak energy as a function of composition was determined. Known quantities of sample powders mixed with MgO were used for the measurements. To obtain information on the local structures, both Fourier transform infrared (FT-IR) (Bruker IFS 113 FTIR spectrometer) and Raman (DILOR RAMAN spectrometer) spectra were recorded. IR spectra were recorded in the range 100−700 cm^{-1} on sample pellets prepared using polyethylene as a binder. Raman spectra were obtained using small, finely polished pieces of glass samples mounted in a backscattering geometry. X-ray absorption near edge spectra (XANES) associated with L_{III} edge of Pb in $Pb_xGe_{42-x}Se_{58}$ glasses were recorded at room temperature on a Rigaku spectrometer (Ru−200B, Rigaku, Japan). The source of X-rays is a rotating anode X-ray tube and the intensities at the Pb L_{III} edge were not sufficiently high to record still finer features. The XANES of Pb L_{III} edge in Pb, PbSe and PbO_2 were also recorded for comparison under identical conditions. Films were made using fine powders of glass samples and polyethylene, and they were used for the XANES measurements. Thickness of the films and the amount of sample taken were so adjusted as to give about twice the absorption lengths of Pb (material needed to get the best spectra was found to be 15 mg cm^{-2} of the film). The effect of pressure on the resistivity of $Pb_xGe_{42-x}Se_{58}$ glasses was studied using a Bridgman opposed anvil (made of tungsten carbide) system[41] up to 8 GPa. Pyrophillite was used as the gasket material and steatite as the quasi-hydrostatic pressure transmitting medium. An in situ pressure calibration was achieved using Bi (pressure transitions of Bi are well-known) in the high-pressure experiments.[42] There was no variation of the temperature of the sample under pressure as monitored using an in situ Cr/Al thermocouple.

3. Results and Discussion

3.1. Structure and Composition. The composition of the glasses investigated in this work are given in Table 1. The glasses were all X-ray amorphous, and the electron micrographs also confirmed their amorphous nature. High resolution electron micrograph of a glass is shown in Figure 1, and there is no evidence of any distinguishable micro structure. The electron diffraction pattern given in the inset to Figure 1 reveals only a weak hollow confirming the noncrystalline nature of the material. The chemical compositions of the glasses were confirmed from EDAX. For example, while the notional (starting material) composition was $Pb_{15}Ge_{27}Se_{58}$, EDAX analysis of the glass composition was $Pb_{14.8}Ge_{26.3}Se_{58.9}$. There was no evidence of any Si in EDAX, confirming that there was no reaction of the silica tube with the contents.

3.2. Densities and Molar Volumes. The densities and molar volumes of the Pb−Ge−Se glasses are shown in Figure 2. All molar quantities in this paper refer to a hundreth of the

TABLE 1: Thermal Properties of Pb−Ge−Se Glasses[a]

composition	T_g (K)	T_c (K)	$(T_c - T_g)/T_g$	C_p at $(T_g - 30)$ K (J K^{-1} mol^{-1})	ΔC_p (J K^{-1} mol^{-1})
$Ge_{42}Se_{58}$	626	777	0.241	28.7	15.7
$Pb_5Ge_{37}Se_{58}$	520, 617	711	0.367, 0.166	27.8, 34.7	7.6, 16.6
$Pb_{10}Ge_{32}Se_{58}$	530	667	0.258	29.8	15.9
$Pb_{15}Ge_{27}Se_{58}$	537	658	0.225	29.7	17.5
$Pb_{20}Ge_{22}Se_{58}$	547	634	0.159	26.3	17.4

[a] Dulong−Petit value of $C_p = 25.1$ J K^{-1} mol^{-1}.

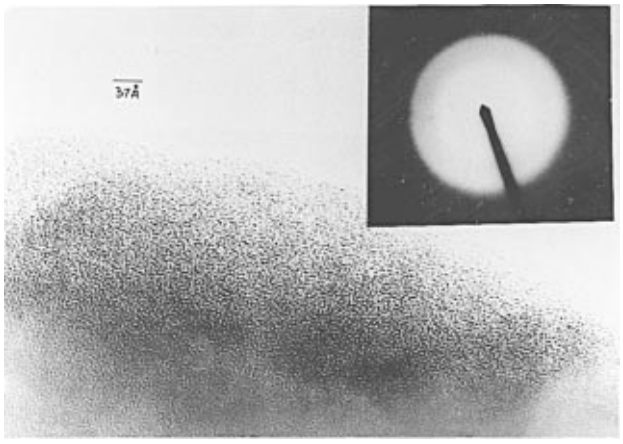

Figure 1. HREM image of $Pb_5Ge_{37}Se_{58}$ glass. The inset gives the electron diffraction pattern of the same.

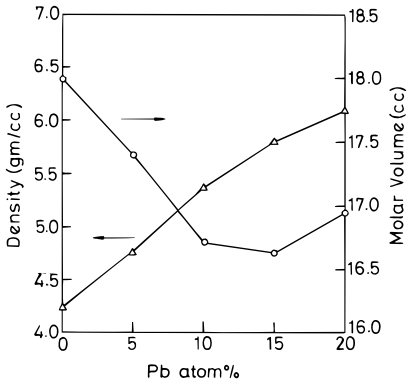

Figure 2. Densities and molar volumes of $Pb_xGe_{42-x}Se_{58}$ glasses as a function of composition.

value for the 100 atom molecule. It is remarkable that, while substitution of Pb for Ge leads to an increase in density of about 50%, molar volume itself changes only a little over 5% (about 1.33 cm^3 over an average of 17.3 cm^3). It is observed that substitution of the larger Pb atoms (atomic radius 1.75 Å) for the smaller Ge atoms (atomic radius 1.37 Å) gave rise to an over all decrease in molar volume. It is therefore suggestive of a collapse of the open structure, since tetrahedrally bonded germanium and two coordinated selenium atoms are systematically substituted by octahedrally coordinated Pb atoms and singly coordinated (and charged) Se atoms (see later).

3.3. Thermal Properties. Glass transition temperatures (T_g's) of the glasses are shown in Figure 3. Line has been drawn through the points only as a guide to the eye. T_g initially decreases rapidly with increasing lead content and changes very little above 7−8 atom % of Pb. Only one composition ($Pb_5Ge_{37}Se_{58}$) exhibited two glass transitions. This feature was reproducible with different preparations of the same composition. Other sample compositions did not exhibit this feature. From Figure 3 it is suggestive that the glass could be phase separated into two glasses one, Ge-rich and the other Pb-rich; the higher T_g could be due to $Ge_{42}Se_{58}$ glass (as easily identified

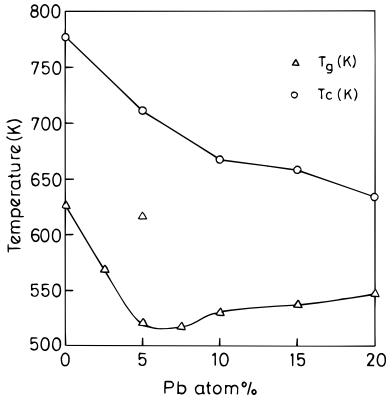

Figure 3. The glass transition (T_g) and crystallization temperatures (T_c) of Pb−Ge−Se glasses as a function of Pb content.

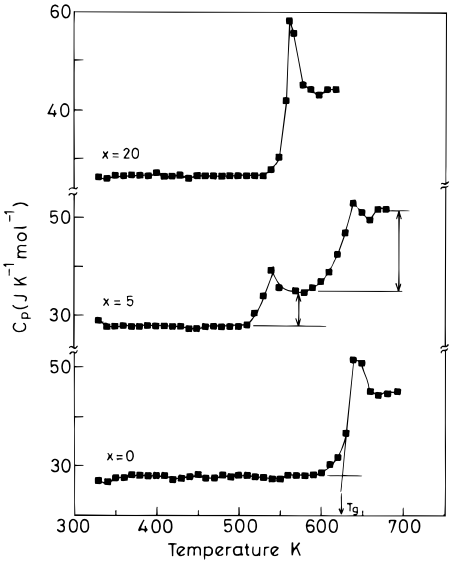

Figure 4. The variation of heat capacities of representative $Pb_xGe_{42-x}Se_{58}$ glasses with temperature.

from Figure 3) while the lower T_g could be due to the Pb-rich composition. The variation of the heat capacities of the various glass compositions as function of temperature are shown in Figure 4. It may be seen from Figure 4b that in $Pb_5Ge_{37}Se_{58}$ glass the two transitions 1 and 2 occur at 520 and 617 K, respectively and that the strengths of these transitions measured as C_p amplitudes are in the ratio 1:2. Transition 2 actually corresponds to T_g of the pure $Ge_{42}Se_{58}$ glass. The magnitude of ΔC_p is generally indicative of the nature of bonding and is generally higher for ionic glasses and lower for covalent ones.[43] The ionicity is determined by the two heteroatom bonds Ge−Se and Pb−Se in the present system of glasses. Since the electronegativities of Pb and Ge are very similar we may assume that the nature of bonding in the phase separated glasses is of similar ionicity. We may therefore make the assumption that magnitudes of ΔC_p represent the proportions of the $Ge_{42}Se_{58}$ and the Pb-rich glass. The composition of the Pb-rich glass

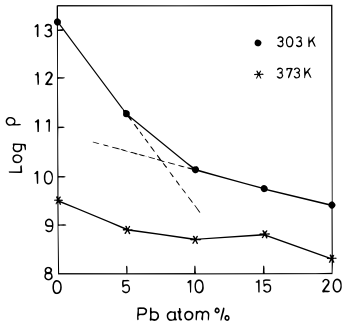

Figure 5. Change in electrical resistivity of Pb−Ge−Se glasses as a function of composition.

itself is then easily identified. The second transition (T_{g_2}) corresponds to that of $Ge_{42}Se_{58}$. Therefore, one component of the phase separated glass is $Ge_{42}Se_{58}$ (or equivalently $Ge_{37}Se_{51}$). The glass composition can be expressed in terms of ($Ge_{37}Se_{51}$) as ($Ge_{37}Se_{51}$)·(Pb_5Se_7). The composition of phase separated glass can be expressed as [x($Ge_{37}Se_{51}$)] [(1 − x) ($Ge_{37}Se_{51}$)·(Pb_5Se_7)], which expresses the fact that only a fraction x of the lead-free glass has separated out and the other fraction is present in the lead-rich part of the glass. The two fractions are in the ratio 2:1 in the order in which they are written in the formula above. Thus ($Ge_{37}Se_{51}$) present in the two phases is in the same ratio requiring $x/(1 - x) = 2/1$ or $x = 0.66$. Thus the phase separated glass is [0.66($Ge_{37}Se_{51}$)][0.33 ($Ge_{37}Se_{51}$)·(Pb_5Se_7)], which is equivalently 0.58[$Ge_{42}Se_{58}$] and 0.42[$Pb_{12}Ge_{30}Se_{58}$]. The T_g of a glass corresponding to the composition $Pb_{12}Ge_{30}Se_{58}$ is expected to be 530 K from Figure 3 by interpolation, and it is gratifying to note that it agrees very well with the observed value. The phase separation observed in 5% Pb glass does not seem to affect the general trends observed in other properties. Therefore no special importance is attached in the discussions to follow on this particular feature occurring in only one composition. Also no attempt was made to characterize the structures of the separated phases of the $Pb_5Ge_{37}Se_{58}$ glass or their crystallized products. Heat capacities of the glasses above laboratory temperature remain nearly constant and are somewhat higher than the Dulong−Petit heat capacity (25.10 J/mol/°C). If the excess heat capacity is assumed to be due to frozen configurational entropy, then it is implied that a significant amount of configurational entropy is frozen in at the T_g of these glasses. The ΔC_p values are uniformly high and do not exhibit significant dispersion (except for the first transition in the 5 atom % lead glass). This is again indicative of the fact that the nature of bonding remains unaltered in these glasses. It may be noted that almost constant heat capacities attained by these glasses is indicative of their Debye temperatures being lower than 300 K. The dispersion in T_g, however, is high and occurs mostly in compositions with under 8 atom % of Pb; above this percentage of Pb, T_g varies very little. The crystallization temperatures, T_c's, (corresponding to the onset of crystallization) are given in Table 1 along with other thermal data. The trend in their variation is similar to those of T_g, although they do not become quite as insensitive to composition variation in high Pb compositions. Stabilities of the glasses[44] inferred from the index ($T_c - T_g/T_g$) are listed in Table 1. Glass stabilities are indicated by the index magnitudes.

3.4. Electrical Properties. The logarithm of resistivities of the glasses at 303 and 373 K are shown in Figure 5 as a function of the concentration of Pb atoms. There is a gradual decrease in the resistivity at 303 K, while the resistivity exhibits a plateau like character at 373 K. The composition dependence of room-temperature resistivity appears to have two different slopes which changes in the region of about 8 atom % Pb.

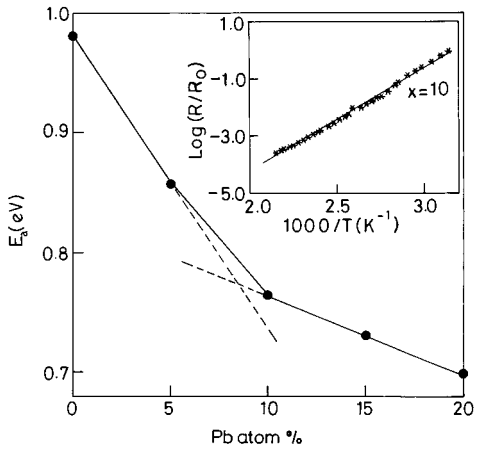

Figure 6. Variation of conductivity activation energy (E_a) with Pb concentration in $Pb_xGe_{42-x}Se_{58}$ glasses. Inset shows a typical semi-logarithmic Arrhenius plot used for the determination of E_a.

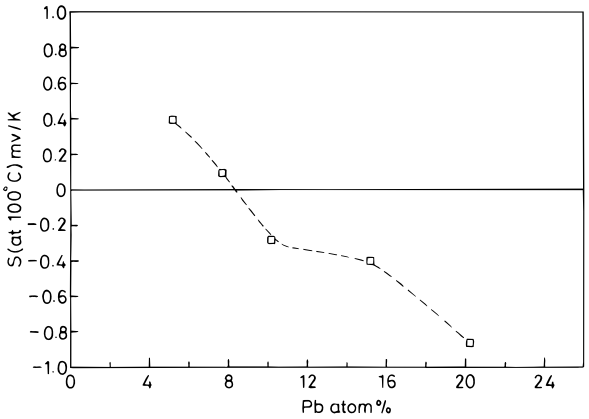

Figure 7. Plot of thermoelectric power S at 373 K for $Pb_xGe_{42-x}Se_{58}$ glasses as a function of composition (line is drawn as a guide to the eye).

Activation energies for the conductivity have been determined for various glass compositions and the variation of E_a with Pb concentration is shown in Figure 6. The inset to Figure 6 is illustrative of the Arrhenius plots used for the determination of the activation barriers. Activation energy variation also shows a break around 8 atom %, with Pb rich glasses exhibiting a slower decrease of E_a as a function of lead concentration. The activation energy of pure $Ge_{42}Se_{58}$ glass (0.987 eV) is in good agreement with the literature reports (0.991 eV).[45] With the introduction of Pb in the place of Ge the semiconducting nature of the glass itself is not affected although the barrier decreases significantly. The results of thermoelectric power (TEP) measurements are presented in Figure 7 as S (Seebeck coefficient recorded at 373 K) vs Pb atom %. It may be noted that around 8 atom % of Pb the Seebeck coefficient changes sign and becomes negative. An important issue addressed in this paper is this transition in the nature of the dominant charge carriers in the Pb−Ge−Se glasses. In a large number of chalcogenide glasses the sign of the Seebeck coefficient is positive indicating that "holes" are the majority charge carriers. It is also known that chalcogenides are characterized by the presence of charged defect pairs of the type C_3^+ and C_1^- where C is identically the chalcogen and is Se in the present case. The subscript to C represents the number of covalent bonds by which Se is connected to other atoms and superscript is the formal charge on the selenium. We may consider the over-coordinated Se_3^+ as a hole-bearing atom (because in reality the dative bond of Se decreases effectively the actual number of electrons in its valence shell by unity as a consequence of

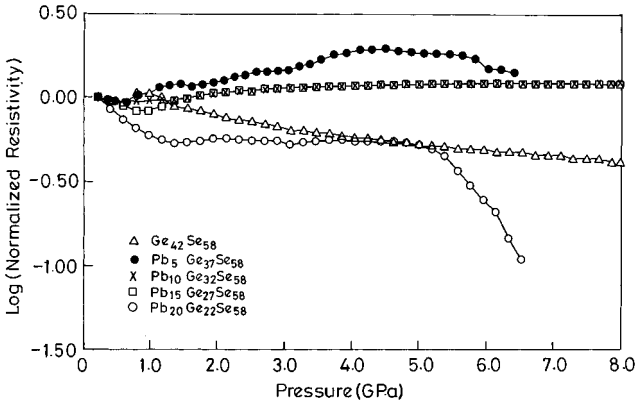

Figure 8. Effect of pressure on the normalized electrical resistivities of Pb−Ge−Se glasses.

sharing with the atom to which it is bonded). Therefore, hole current in these glassy chalcogenides can be thought of the motion of these C_3^+ centers. This motion occurs in a fairly facile manner through a bond-switching mechanism utilizing the nearby C_2 centers:[46]

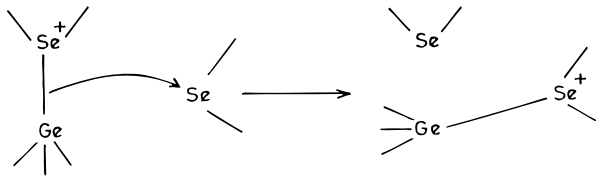

Transferring C_1^- centers, on the other hand, in the glassy matrix is not considered as facile. This in general leads to a p-type conduction although in reality transport in chalcogenide glasses is ambipolar.[35] Suppression of the concentration of C_3^+ centers and enhancement of C_1^- as a consequence of replacing Ge by Pb can therefore be considered as a possible origin of the charge carrier sign reversal. We will see later that this approach is not adequate. Resistivities of $Pb_xGe_{42-x}Se_{58}$ glasses were also measured as a function of pressure at laboratory temperature. In Figure 8 the variation of the normalized resistivities as a function of pressure are given in a semilogarithmic plot. In general, the pressure dependency of resistivity is very low for all the glasses. There is no pressure induced transition except perhaps in $Pb_{20}Ge_{22}Se_{58}$ glass. There is a pronounced drop in resistivity which may be attributed to the onset of crystallization but we have not been able to confirm the transition to crystalline state on the basis of XRD data. Most remarkably, glasses close to the charge reversal transition region exhibit resistivities almost independent of pressure up to 8 GPa. This implies absence of any influence of pressure on the charge transport and suggest that charge transport is associated with such energy levels (atomic or molecular orbitals) which are structurally so shielded that external pressure does not perturb them. We will discuss this aspect in a later section.

3.5. Spectroscopic Investigations. Diffuse reflectance spectra (DRS) and variation of optical energy gaps obtained from the peak maximum energies in DRS as a function of Pb concentration are shown in Figure 9 and its inset, respectively. Optical gaps are found to be uniformly more than twice of the gaps calculated from the conductivity data and bear no simple (ratio type) relation with E_a. Further diffuse reflectance peaks are rather broad suggesting that the energy bandwidths of both valence and conduction states are very broad. However, a plateau-like composition insensitivity is seen around the region of p → n transition in the DRS energies which is similar to the behavior seen in Bi−Ge−Se glasses.[47] The far-infrared spectra

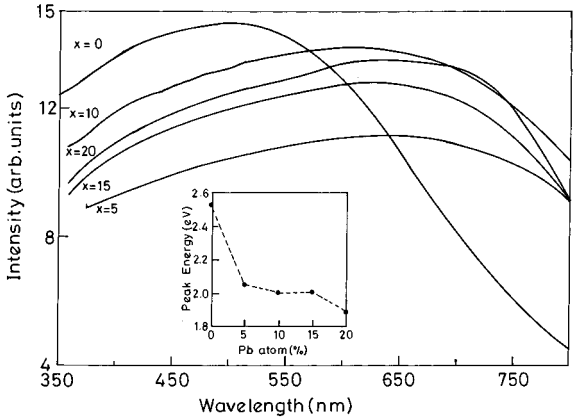

Figure 9. Diffuse reflectance spectra (DRS) of lead−germanium-selenide glasses as a function of composition. The inset gives the variation of DRS peak maximum energy as a function of Pb content.

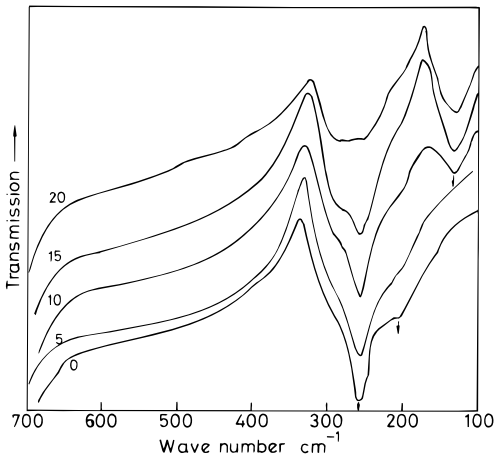

Figure 10. Infrared spectra of $Pb_xGe_{42-x}Se_{58}$ glasses as a function of Pb concentration.

of the glasses are given in Figure 10. The 255 cm^{-1} asymmetric stretching in the IR confirms the presence of $GeSe_{4/2}$ units in the glass structure.[48] The shoulder around 207 cm^{-1}, which is absent in Pb rich compositions, is likely to be due to the bending mode associated with Ge−Ge−Ge type of links which we will see later could be present in Ge-rich glasses. The emergence of 130 cm^{-1} feature as a fairly intense mode in Pb-rich (≥10%) glasses is associated with the vibrational mode of a [$PbSe_6$]-distorted octahedra. The 130 cm^{-1} mode is present dominantly in crystalline PbSe spectra also.[48] It may be noted that the intensity of this peak increases as the concentration of Pb increases. Coincidentally, the 255 cm^{-1} peak broadens and exhibits a shoulder like feature associated with it. The latter can be attributed to the vibrations of a chemically distinct but tetrahedrally coordinated Ge which is formed in Pb containing glasses. Raman spectra of the glasses are presented in Figure 11. The most important features in the spectra are the peaks at 174 and 198 cm^{-1}, both of which are associated with Ge in tetrahedral position but the former with ethylenic[49,50] $Ge_2(Se_{1/2})_6$. The other somewhat broad scattering centered around 286 cm^{-1} is associated with the presence of Ge−Ge phonon mode in glasses. Both the 174 cm^{-1} ethane-like mode and 286 cm^{-1} phonon mode gradually decrease in intensity and vanish as Pb content is increased from 0 to 20 atom %. On the other hand, 198 cm^{-1} Raman mode associated with $GeSe_{4/2}$ increases in intensity with respect to the other two modes and is the only mode observed in $Pb_{20}Ge_{22}Se_{58}$ glass. Thus the FTIR and Raman spectra together confirm that Ge and Pb in the present glass system are present, respectively, in tetrahedral and

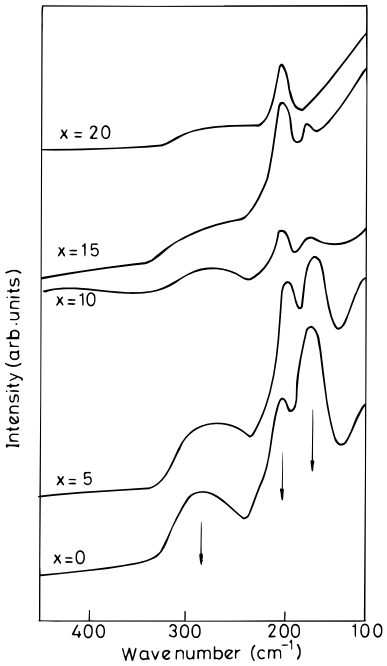

Figure 11. Raman spectra of $Pb_xGe_{42-x}Se_{58}$ glasses.

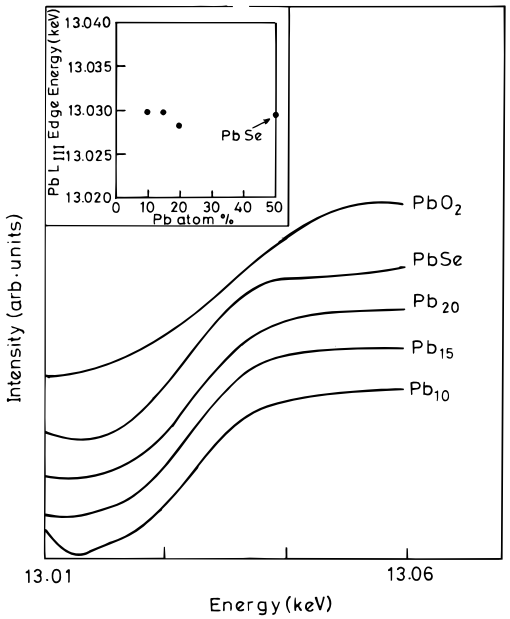

Figure 12. X-ray absorption near edge spectra associated with the Pb L_{III} edge of Pb−Ge−Se glasses. XANES spectra of crystalline PbSe and PbO_2 is also given for comparison. The absorption edge energies are plotted in the inset as a function of Pb atom %.

octahedral coordinations only. The above spectroscopic features are utilized in the following section to propose a structural model for these glasses. The X-ray absorption near edge spectra (XANES) associated with the L_{III} edge of Pb in $Pb_xGe_{42-x}Se_{58}$ glasses are presented in Figure 12 along with those of crystalline PbSe and PbO_2. The energies corresponding to the points of inflection on the absorption edges have been plotted in the inset to Figure 12 with the *X*-axis representing Pb atom %. The comparison clearly establishes that Pb is situated in octahedral environment of Se, much as in crystalline PbSe. Neither in glass nor in crystalline PbSe do we observe any pronounced white-line-like intensity at the edge, and the absence of such edge feature indicates that the nature of bonding of the Pb atom is significantly ionic. Further, the spectra also confirm that Pb is present as Pb^{2+} only[31,32] and not Pb^{4+}.

TABLE 2: Number of Different Types of Bonds Present in Pb−Ge−Se Glasses

composition	*n*b-Se	b-Se	Pb−Se	Ge−Se	Ge−Ge
$Ge_{42}Se_{58}$	0	58	0	116	26
$Pb_5Ge_{37}Se_{58}$	10	48	10	106	21
$Pb_{10}Ge_{32}Se_{58}$	20	38	20	96	16
$Pb_{15}Ge_{27}Se_{58}$	30	28	30	86	11
$Pb_{20}Ge_{22}Se_{58}$	40	18	40	76	6

3.6. Structural Model. On the basis of vibrational spectra and XANES, we assume that Ge is always tetrahedrally coordinated and Pb octahedrally coordinated in the present glass system. An occasional defect such as 3- or 6-coordinated Ge or a 4-coordinated Pb are completely ignored. The Pb free composition of $Ge_{42}Se_{58}$ can be built starting from tetrahedrally coordinated 3-dimensional amorphous Polk like germanium structure.[51] The lattice would consist of $42(^4/_2) = 84$ Ge−Ge bonds. The selenium atoms are incorporated into the structure by inserting 58 cuts randomly among the 84 Ge−Ge bonds. Since the initial glass is a germanium excess composition in relation to $GeSe_2$, we assume (a chemically ordered network model) that there are no Se−Se bonds, absence of which is also consistent with the vibrational spectra in Figures 10 and 11. Thus the $Ge_{42}Se_{58}$ glass would consist of bridging Se (b-Se) and Ge−Ge bonds. In fact, since out of 84 Ge−Ge bonds 58 has been used-up, the remaining 26 Ge−Ge bonds have to be shared by the 42 Ge atoms. Since 26 is greater than $^{42}/_2$, Ge−Ge bonds are not isolated from each other and hence there will be Ge−Ge−Ge bonds as well. It is the presence of these which are responsible for the pronounced broad humplike feature in Raman spectra around 286 cm^{-1} (phonon mode). The structures of Pb−Ge−Se glasses are also generated in a similar manner. Since *n*Pb atoms are present as Pb^{2+} ions, in a $Pb_nGe_{42-n}Se_{58}$ glass there are 2*n* *n*b-Se atoms. Therefore there are $(58 - 2n)$ b-Se atoms. Number of cuts to be made in a lattice of $(42 - n)$ Ge atoms, which has $(84 - 2n)$ Ge − Ge bonds, is equal to $(58 - 2n + 2n/2)$ or $(58 - n)$. Since $(84 - 2n) \geq (58 - n)$ for $n \leq 26$, the situation is least complicated because *n* in our glasses does not exceed 26. Into first *n* random cuts Se atoms are inserted in pairs and attached singly to the Ge atoms. These are designated as *n*b-Se atoms. They other $(58 - 2n)$ cuts receive the remaining $(58 - 2n)$ b-Se atoms. The tally of *n*b-Se, b-Se, Ge−Se, and Ge−Ge bonds present in the various glass compositions are listed in Table 2. Pb^{2+} ions are randomly inserted into the structure so that they settle in positions where they are surrounded by six seleniums of which at least one or two of them are *n*b-Se's. Such a system is further assumed to be as relaxed and equilibrated. Because of the *n*b-Se's and 6-coordinated Pb^{2+} ions, the glass becomes systematically more compact and therefore the volume is expected to decrease which is quite consistent with Figure 2.

3.7. Charge Transport in Chalcogenides. Charge transport in chalcogenide glasses is known to occur through the participation of charged defects.[52] In the binary Ge−Se glass, where no *n*b-Se has been introduced by the presence of modifying PbSe, charged defect pairs of the following types are formed:

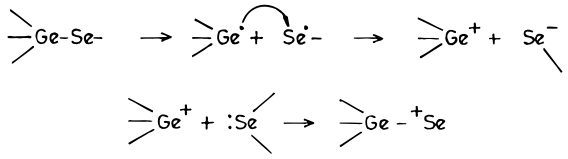

The net result is formation of singly bonded negatively charged Se_1^- and three bonded positively charged Se_3^+. The

formation of charged defects is quite general and is represented as

$$2\,C_2^{o} \rightleftharpoons C_1^{-} + C_3^{+} \rightarrow (1)$$

where C represents a chalcogen and the subscript is its coordination number. It may be noted that, in the above "reaction", which leads to the formation of charged defect pairs from normal neutral covalently linked selenium atoms in the structure, the total number of covalent bonds are conserved and the net energy of the reaction corresponds to the energy of pairing of the electrons in a p (or sp_n; $n = 1-3$) orbital, which is denoted as U_{LP}. In glasses where several other bonds are present, notably when another chalcogen is present, a weaker bond is broken and a stronger bond is formed so that the net energy expected in the defect pair creation process is reduced from U_{LP} to $U_{LP} - \Delta E$, where ΔE is the energy difference between the stronger and weaker bonds. Any other associated stabilizing factors will correspondingly reduce the net energy of the reaction which we shall call as modified pairing energy, U'_{LP}. We have shown earlier[52] that the activation barrier for dc conductivity in chalcogenide glasses is actually equal to the U'_{LP} in chalcogenide glasses. It is strongly suggestive of a transport mechanism similar to charge transport through defects in alkali halides except for the migration barrier (as if in the extrinsic region). The activation barrier in the binary $Ge_{42}Se_{58}$ glass is ≈0.987 eV and is consistent with activation barriers found in a variety of other selenide glasses. The nature of the defect pair will remain the same in all glass compositions. When Pb is introduced into the glasses, C_1^- defects, which are identical with *n*b-Se, are created and their concentration is equal to that of Pb itself. *n*b-Se's tend to be present always in the coordination polyhedra of Pb^{2+} because of colombic attraction. The lone pair of Se_1^- is stabilized due to strong polarization by Pb^{2+} ions as a result of which the net energy for defect pair formation in eq 1 is reduced. The effective lone-pair formation energy U'_{LP} thus involved is found to be approximately equal to E_a, the dc activation barrier. This stabilization energy increases with the increasing Pb^{2+} ions in the system because Se_1^- experiences the influence of greater number of Pb^{2+} ions. However, the stabilizing influence is "off-set" at higher concentration of Pb^{2+} by the inter Se_1^- colombic repulsion. Therefore, we expect that as a function of Pb concentration U'_{LP} decreases steeply at lower Pb concentration and less markedly at higher Pb concentrations. The observed trend of E_a ($\approx U'_{LP}$) in Figure 6 supports the above approach. The defect pair equilibrium in chalcogenide glasses is governed by an equilibrium constant, *K*, which may be written as

$$K = [C_3^{+}][C_1^{-}]/[C_2^{o}]^2 = [[C_3^{+}]/[C_2^{o}]]*[[C_1^{-}]/[C_2^{o}]] \quad (2)$$

Values of $[C_1^-]/[C_2^o]$ which is nearly equal to [*n*b-Se/b-Se] which can be calculated in compositions containing Pb, because intrinsic C_1^- concentration as in lead-free chalcogenides is very small and can be ignored. These values are given in Table 2. It may be noted from Table 2 that $[C_1^-]/[C_2^o]$ changes from 0.21−2.22 as the Pb atom concentration increases from 5−20. The increase in $[C_1^-]/[C_2^o]$ by an order of magnitude suggests that $[C_3^+]/[C_2^o]$ decrease by the same factor of 10 in this regime of composition as required by eq 1. By the same argument we would expect that $[C_1^-]/[C_3^+]$ to vary by roughly 2 orders of magnitude over the same range of compositions. From the relation,

$$K \approx \exp(-\Delta G/RT) \approx \exp(-\Delta E/RT) \quad (3)$$

where ΔG and ΔE are free energy and formation energy, respectively, for the reaction in eq 1, one can determine *K* since $\Delta E \approx U'_{LP} \approx E_a$ the experimental dc activation barrier. *K* is expected to increase with increasing percentage of Pb since E_a decreases. Therefore, the numbers of $[C_3^+]$ and $[C_1^-]$ also increase in addition the ratio $[C_1^-]/[C_3^+]$. Motion of both C_3^+ and C_1^- type of defects are considered to contribute to the conductivity. It is easy to visualize motion of C_3^+ type of defects, which is accomplished by the switching of a bond between $[C_2^o]$ and $[C_3^+]$; $[C_2^o] + [C_3^+] \rightleftharpoons [C_3^+] + [C_2^o]$, compared to C_1^-. In the region of low Pb concentration C_3^+ can be assumed to act as the major charge carrier and the glasses are p-type. But as their concentration decreases rapidly with increase in Pb, with a corresponding increase in C_1^- at higher concentrations of Pb, C_1^- centers can be expected to become dominant charge carriers which therefore results in carrier sign reversal to n-type. Since the decreasing value of E_a tries to push up the concentration of $[C_3^+]$, the transition to n-type as a function of composition is somewhat gradual. This may be contrasted with the behavior of $Pb_{20}Ge_ySe_{80-y}$ glasses discussed in the literature.[38] In the latter glasses an increase in activation barrier has been reported[38] as a function of increasing Ge content ($y = 19-23$). This increase in E_a is actually due to decrease in Se content and decreases $Se^- - Se^-$ distances and it leads to a sharp decrease of C_3^+ and increase of C_1^-, which makes the experimentally observed p → n transition also sharp with respect to composition variation. However, change of carrier type should be dependent on the mobilities also. The experimental mobilities for electrons and holes in these chalcogenides have been reported to the rather similar.[33] We therefore expect $[C_3^+]$ and $[C_1^-]$ concentrations to be not too dissimilar in magnitude in the crossover region. But in the above model $[C_3^+]/[C_2^o]$ is expected to be around $10^{-13}-10^{-15}$ while $[C_1^-]/[C_2^o]$ is of the order of unity. Therefore the model cannot rationalize the observed p → n transition. We therefore use below a band structure approach to examine the problem of p → n transition.

3.8. Energy Band Structure of Pb−Ge−Se Glasses. The electronegativities of Pb and Ge are very similar. Therefore Pb^{2+} may be expected to pull sufficient electron density around itself in the bonded state in the glass. Since experimentally (see section on spectroscopy) Pb is found to be in octahedral coordination, Pb is assumed to be in a sp^3d^2 state of hybridization. Se atoms are in sp^n ($n = 1$, 2, and 3) hybridization, and the lone pairs on several of them are highly polarized toward Pb^{2+} ions. Germanium is tetrahedrally bonded and it utilizes its sp^3 hybridized orbitals for bond formation. We construct an approximate band energy diagram which is shown in Figure 13. The lowest energy levels result from the overlap of the bonding orbitals. The Ge−Se bonding in $GeSe_{4/2}$ units or in mixed coordination units such as ($Ge_{1/4}Se_{3/2}$), give rise to four bonding orbitals which possess the full requirement of eight electrons from the participating Ge (4) and Se/Ge (1 × 4) atoms. The Ge−Se and Ge−Ge therefore constitute the lowest energy levels. The next higher energy level is constituted of sp^n lone pairs originating from the selenium. The lone-pair levels of charged Se^- are presumably of slightly higher energy. The sp^3d^2 orbitals on Pb^{2+} ions are likely to occupy a slightly higher level than the selenium lone-pair levels. The bonding is likely to be more complicated than reported in this simple model. One of the orbitals of sp^3d^2 set is filled by two electrons of lead. This situation can be similar to the coordination found in compounds such as $PbGeS_3$,[53] where the lone pair on lead is in effect a steriochemically active lone pair. The limited overlap of empty sp^3d^2 orbitals with the filled sp (lone pair) orbitals of Se may lead to some stabilization reminiscent of bonding stabilization

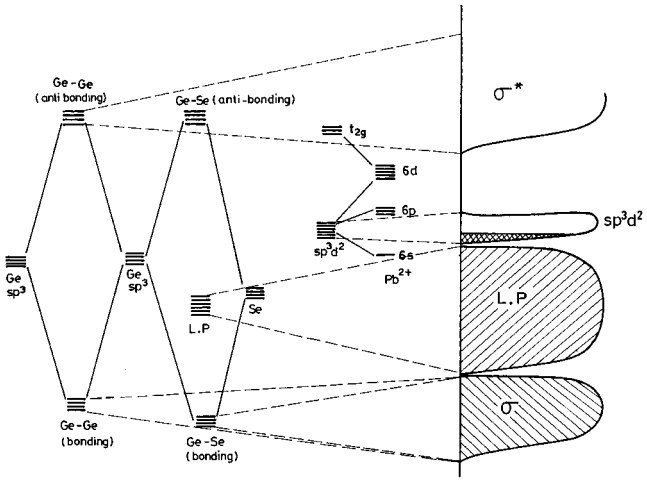

Figure 13. Molecular orbital scheme used for the formation of energy levels and the schematic energy band diagram constructed for $Pb_xGe_{42-x}Se_{58}$ glasses.

in PbO.[54] While the e_g set of d orbitals (in a presumed O_h symmetry) are taken up in the set of sp^3d^2 orbitals, the t_{2g} orbitals of Pb are located in the energy region of the antibonding σ^* levels. The relevant schematics of the energy band diagram are shown in Figure 13. Figure 13 describes the approximate molecular orbital scheme for the formation of energy levels described above and for the energy bands with a schematic density of states. The broad band of Se lone pairs is shown as overlapping with the top portion of the lowest energy band due to Ge−Se and Ge−Ge bonds. The energy levels of Pb are expected in this model to be higher since Pb is found to be ionic Pb^{2+}. We have shown the sp^3d^2 band of Pb^{2+} ions just above and separated from the sp lone-pair levels of chalcogens. The triplet t_{2g} levels of Pb are still higher and overlapping with the empty antibonding σ^* levels. Since the top of the lone pair band is constituted of Se^- or C_1^- type of states, electron transport between C_1^- states via an empty sp^3d^2 state. We will estimate this electronic conductivity contribution later. Increasing Pb concentration leads to rapid growth of both sp^3d^2 band and the C^-_1 states (top of sp band) and hence rapid increase of the electron contribution to conductivity, which can exceed the contribution from holes. As a consequence, a p → n transition ensues as a function of increasing Pb concentration. We would also like to note here that decreasing Ge concentration and the attendant increase in compactness shifts the lone pair band upward in energy, making it even easier for the electron transport.

3.9. Electrical Transport and Carrier-Type Reversal. The total conductivity σ is considered as a sum of $\sigma_h + \sigma_e$ the conductivities due to holes (h) and electrons (e). These contributions are calculated as a product of $n_h\, e\mu_h$ and $-n_e e\mu_e$. n_h is the effective number of holes or the C_3^+ centers involved in transport. To evaluate this number, use was made of the defect model according to which the C_3^+ concentration is approximately,

$$\sqrt{[C_3^+][C_1^-]} \approx n_h \approx [C_2^o]\exp(-E_a/2kT) \qquad (4)$$

where E_a is the experimental dc activation barrier and $[C_2^o]$ is the concentration of bridging seleniums per cm^3. $[C_2^o]$ is calculated from molar volume and composition. However, all the $[C_3^+]$ may not be contributing to conductivity since their motion requires a vicinal and configurationally properly located $[C_2^o]$. To fix the fraction of $[C_3^+]$ involved in charge transport, experimental conductivity of Pb-free glass was utilized. Since in lead-free glass $\sigma_{total} \approx \sigma_h$ itself and since μ_h is known[33] to be $\approx 2 \times 10^{-5}$ cm^2/V s, n_h should be equal to $\sigma/e\mu_h \approx 2.8 \times 10^{10}$ per cm^3. Since n_h obtained from the defect model is (eq 4) $\approx 10^{14}/cm^3$, the effective number of $[C_3^+]$ or holes involved in transport can be taken as

$$n_h = \sqrt{[C_3^+]^*[C_1^-]} \approx 10^{-4}[C_2^o]\exp(-E_a/2kT) \qquad (5)$$

This factor of 10^{-4} is assumed to be a constant for all compositions. Such a procedure ignores effect of increasing concentration of $[C_1^-]$ on $[C_3^+]$ concentrations. The only justification for this is that most $[C_1^-]$ is tied up with Pb^{2+} in the structure through strong polarization and are not involved in the quantities in eq 2. This is perhaps the reason why increased $[C_1^-]$ alone is not really capable of explaining the p → n transition as noted earlier. Thus, on the basis of above analysis, σ_h has been calculated for all the compositions using eq 5. σ_e was calculated on the assumption that electron pairs−bipolarons were transported between two $[C_1^-]$ centers via an intervening sp^3d^2 orbital of a lead atom. It is visualized that the transient state of the pair of electrons in the sp^3d^2 orbital constitutes an activated state; the activation energy being the difference in the pairing energy of electrons in a 4d-mixed orbital of Pb and 4p-dominated orbital of a selenium. The pairing energies are well-known to be higher in d-orbitals ($L = 2$) compared to p-orbitals ($L = 1$). Unfortunately, these pairing energies are not known experimentally. We have used below arbitrary but plausible values of the differences in pairing energies ($\Delta\ U_{LP}$) and evaluated σ_e. Experimental electron mobility is known in one of the glass compositions, and we have approximated the same in all compositions. Thus σ_e was evaluated as

$$(xN/V)\exp(-\Delta U_{LP}/kT)e\mu_e$$

where x is the atom fraction of Pb and hence concentration of C_1^- centers, N is Avogadro number, and V is the molar volume. ΔU_{LP} was treated as composition dependent because the sp^3d^2 bandwidth itself increases with concentration of Pb, thereby decreasing the pairing energy in d-band. All the relevant parameters used in the calculations are listed in Table 3 along with calculated values of the conductivity. In Figure 14, the behavior of the calculated conductivities are shown as function of composition and the total calculated conductivity is compared with the experimentally determined values. Thermopower was evaluated as a conductivity weighted sum of the contributions of electrons and holes to the total thermopower using the expression,

$$S = [\sigma_e S_e + \sigma_h S_h]/[\sigma_e + \sigma_h] \qquad (6)$$

Individual S_h and S_e values were calculated as $S_h = +k/e[E_a/kT + 1]$ and $S_e = -k/e[\Delta U_{LP}/kT + 1]$. We have assumed the relevant activation barriers for holes and electron transport as E_a and $\Delta\ U_{LP}$. We may recall that E_a is the activation barrier for hole motion in the spirit of the defect model and the ΔU_{LP} is the activation barrier which the electrons experience according to the present model. All the calculated thermopowers (S_e, S_h, and S_{model}) are shown as a function of composition in Figure 15 along with the experimentally observed thermopower values ($S_{experiment}$). It is gratifying to note that a carrier sign reversal occurs in the present glass system around 8% Pb. The most important feature is that this model which is built on few plausible assumptions on energy band structure and transport behavior enables a satisfactory resolution of the carrier type reversal in Pb−Ge−Se glasses.

TABLE 3: Calculated Electronic Parameters of $Pb_xGe_{42-x}Se_{58}$ Glasses

composition	n_h cm^{-3}	n_e cm^{-3}	σ_h (S cm^{-1})	σ_e (S cm^{-1})	σ_{exptl} (S cm^{-1})	σ_{model} (S cm^{-1})	ΔU_{LP} (model) (eV)	E_a (exptl) (eV)
$Ge_{42}Se_{58}$	2.02×10^{10}		6.47×10^{-14}		8.96×10^{-14}	6.47×10^{-14}		0.987
$Pb_5Ge_{37}Se_{58}$	2.63×10^{11}	1.00×10^{11}	8.42×10^{-13}	3.21×10^{-13}	5.52×10^{-12}	1.16×10^{-12}	0.61	0.856
$Pb_{10}Ge_{32}Se_{58}$	2.12×10^{12}	4.58×10^{12}	5.19×10^{-12}	1.47×10^{-11}	7.41×10^{-11}	1.99×10^{-11}	0.53	0.764
$Pb_{15}Ge_{27}Se_{58}$	3.14×10^{12}	4.77×10^{13}	1.00×10^{-11}	1.53×10^{-11}	1.77×10^{-10}	1.63×10^{-10}	0.48	0.730
$Pb_{20}Ge_{22}Se_{58}$	5.61×10^{12}	9.18×10^{13}	1.80×10^{-11}	2.94×10^{-10}	3.98×10^{-10}	3.12×10^{-10}	0.47	0.699

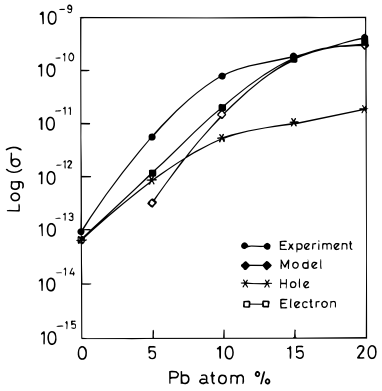

Figure 14. The variation of hole conductivity, electronic conductivity and total conductivity of $Pb_xGe_{42-x}Se_{58}$ glasses calculated using the model as a function of Pb content. The experimentally observed conductivities are also plotted for comparison.

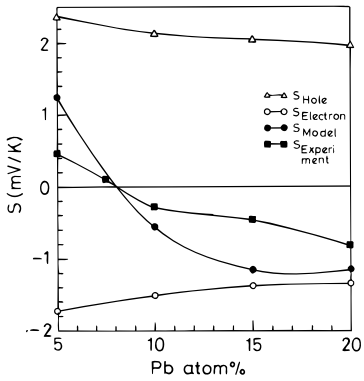

Figure 15. Variation of calculated (using the model) and experimentally observed thermopower values of Pb−Ge−Se glasses as a function of Pb concentration.

3.10. Experimental Observations and the Model. The diffuse reflectance data presented in Figure 9 is consistent with this picture. The photoexcitation of electrons occur from the top of the lone-pair band to the empty antibonding levels. With the increasing concentration of Pb, there will be several competing influences on the energies of the electrons at the top of the lone-pair band. First, stabilization of the electrons at the top of the lone pair band by Pb^{2+} ions (ground-state electron energy is lowered). Second, due to increasing compactness of the glass structure, the lone-pair levels are perturbed and hence their energy raises. Third, increasing concentration of Pb affects the Ge−Se bonds (Ge−Se$^-$ bond is weaker than Ge−Se bond) and thereby increases the width of the antibonding σ^* band, spreading it to lower energy levels. The observed plateau-like variation in the spectra of middle compositions could be the result of the compensating influences of the factors discussed above on the energies of the electrons. This model is consistent with the incidence of p → n transition in $Pb_{20}Ge_ySe_{80-y}$ (y = 17−23) series of the glasses also. The situation in low germanium end of the glass composition ($Pb_{20}Ge_{17}Se_{63}$) is such that the sp^3d^2 band is well above the lone-pair band. This is so because the lone-pair level is made of a significant number of the lone pairs from diselenium units present in this composition (as well as composition up to $Pb_{20}Ge_{20}Se_{60}$). Their energies are therefore located lower on the energy axis, and the bandwidth is also low. The lack of spread is associated with a corresponding increase in the density of states. As the Ge concentration is increased and the composition corresponding to the CTR transition ($Pb_{20}Ge_{21}Se_{59}$) is reached, not only are the Se−Se bonds completely eliminated but also a more compact structure results due to larger number of tetrahedrally bonded centers. This results in significant perturbation of the lone pair levels which spreads the lone pair band upward in energy. The resulting closeness of the sp^3d^2 band with the lone-pair band brings about a dominance of the electron contribution to transport. The trend in conductivity continues toward Ge-rich compositions. Therefore the transition in $Pb_{20}Ge_ySe_{80-y}$ glasses occur by the upward movement of the lone-pair levels, closing in the sp^3d^2 lone-pair bandgap, while in $Pb_xGe_{42-x}Se_{58}$ series CTR occurs as the sp^3d^2 band spreads, bringing about a decrease in the gap to similar level. It may be noted that the absolute values of the lower end of the sp^3d^2 band and the upper edge of the lone-pair band are not the same in the two series of the glasses and the that phenomenon depends only on the energy gap. It is noted that the band description proposed here depends on (i) utilization of the sp^3d^2 band of Pb and (ii) composition dependent variation of band energies, so that both electrons and holes originate from very similar energy levels. The numbers of both holes and electrons are therefore determined by the Pb concentration and are similar if not equal in magnitude. The total concentration of holes and electrons increase with lead concentration. The resistivity data in Figure 5 is consistent with this because not only are the high Pb compositions are n-type semiconductors, but their resistivities are lower. The effect of pressure on the structure of these glasses is experienced mostly as bond deformations. Therefore, only the bridging seleniums and particularly those connected with tetrahedrally coordinated Ge are affected by pressure because they are the most flexible parts of the glass structure. As a consequence, the energy levels associated with Pb in the structure are left unperturbed. The top of the lone-pair band, which is constituted of *n*b-Se's, also remain unaffected. Together they will leave the electronic transport in these glasses unaffected by pressure as observed experimentally. However, when the Pb concentration is as high as 20% or more and the ratio of [*n*b-Se/b-Se] is high, then the sp^3d^2 band can be expected to respond to pressure. Increase in the width of the sp^3d^2 band is expected to occur, which increases the conductivity of the glass. This is also consistent with the pressure behavior of resistivity shown in Figure 8. Only Pb and Bi containing germanium chalcogenides are known to exhibit p → n transition. This unique behavior can be associated with the unique tendency of Pb and Bi toward octahedral coordination and, more importantly, with the energetic disposition of their d-bands which can overlap in energy with those of lone-pair bands of selenium in particular. One can visualize that, even when the coordination of bismuth is low,[29] the lone-pair band can still be found to be close in energy to at least one of the d-bands formed by the splitting of the d levels in the low symmetry of the surrounding Se polyhedron. A situation similar to the one discussed above will be created and the ambipolar

conduction becomes dominated by electron transport at higher percentages of Bi. None of the electrical measurements performed on $Pb_5Ge_{37}Se_{58}$ glass revealed any anomalies which could be attributed to phase separation. The two phases had the compositions $Ge_{42}Se_{58}$ (58%) and $Pb_{12}Ge_{30}Se_{58}$ (42%) and were respectively p and n type semiconductors. The proportions are therefore not too dissimilar in magnitude and well above the percolation thresholds for both the phases to establish their individual connectivities in the structures. We only speculate here that it is fortuitous that the sum of the contributions of these phases to both conductivity and thermopower have been the same as that expected for a homogeneous glass of composition $Pb_5Ge_{37}Se_{58}$. It is likely that this phase separation manifests more noticeably in ac electrical measurements.

4. Conclusions

The phenomenon of carrier type reversal in Pb modified germanium chalcogenide glasses has been investigated and a model has been proposed to account for the occurrence of CTR. The thermal, electrical, and spectroscopic properties of the Pb−Ge−Se glasses which exhibit significant changes across the p → n transition as a function of composition have also been successfully explained using the model. Pb is found to be octahedrally coordinated and the incorporation of Pb significantly alter the electronic band structure and the energetic disposition of the Pb sp^3d^2 band. The closeness of the sp^3d^2 band with those of the lone pairs of chalcogen is suggested to be responsible in bringing about the conduction type reversal.

Acknowledgment. The authors thank Prof. A. K. Sood and Dr. T. Arunarkavalli of the Indian Institute of Science for their help. One of the authors (B.V.) thanks the European Commission for financial support.

References and Notes

(1) Lathrop, D.; Eckert, H. *J. Phys. Chem.* **1989**, *93*, 7895.
(2) Rao. K. J.; Mohan, R. *J. Phys. Chem.* **1980**, *84*, 1917.
(3) Asokan, S.; Prasad, M. V. N.; Parthasarathy, G.; Gopal, E. S. R. *Phys. Rev. Lett.* **1989**, *7*, 808.
(4) Rao, K. J.; Balasubramanian, S. *J. Phys. Chem.* **1994**, *98*, 9216.
(5) Kolobov, A. V.; Elliott, S. R. *Adv. Phys.* **1991**, *40*, 625.
(6) Street, R. A.; Mott, N. F. *Phys. Rev. Lett.* **1975**, *35*, 1293.
(7) Mott, N. F.; Davis, E. A.; Street, R. A. *Philos. Magn. B* **1975**, *32*, 96.
(8) Kastner, M.; Adler, D.; Fritzsche, H. *Phys. Rev. Lett.* **1976**, *37*, 1504.
(9) Tohge, N.; Yamamoto, Y.; Minami, T.; Tanaka, M. *Appl. Phys. Lett.* **1979**, *34*, 640.
(10) Tohge, N.; Minami, M.; Tanaka, T. *J. Non-Cryst. Solids* **1980**, *38,-39*, 283.
(11) Kumar, S.; Kashyap, S. C.; Chopra, K. L. *J. Appl. Phys.* **1992**, *72*, 2066.
(12) Kounavis, P.; Mytilineou, E. *J. Non-Cryst. Solids* **1996**, *201*, 119.
(13) Tichy, L.; Ticha, H.; Pacesova, A.; Petzlt, J. *J. Non-Cryst. Solids* **1991**, *128*, 191.
(14) Bhatnagar, V. K.; Bhatia, K. L.; Yadav, V.; Kishore, N. *Phys. Rev. B* **1989**, *39*, 11203.
(15) Bhatia, K. L.; Gosain, D. P.; Parthasarathy, G.; Gopal, E. S. R. *Phys. Rev. B* **1986**, *34*, 8786.
(16) Phillips, J. C. *Phys. Rev. B* **1987**, *36*, 4265.
(17) Agnihotri, A. K.; Kumar, A.; Nigam, A. N. *J. Non-Cryst. Solids* **1987**, *93*, 267.
(18) Elliott, S. R. In *Disordered Semiconductors*; Kastner, M. A., Thomas, G. A., Ovshinsky, S. R., Eds.; Plenum: New York, 1987; p 219.
(19) Ovshinsky, S. R. In *Amorphous and Liquid Semiconductors*; Spear, W. L., Ed.; University of Edinburgh: Edinburgh, 1977; p 519.
(20) Tohge, N.; Kanda, K.; Minami, T. *Appl. Phys. Lett.* **1986**, *48*, 1739.
(21) Kounavis, P.; Mytilineou, E.; Roilos, M. *J. Appl. Phys.* **1989**, *66*, 708.
(22) Bhatia, K. L. *J. Non-Cryst. Solids* **1983**, *54*, 173.
(23) Polcik, M.; Drohokupil, J.; Drbohlav, I.; Tichy, L. *J. Non-Cryst. Solids* **1995**, *192,193*, 380.
(24) Nagels, P.; Tichy, L.; Triska, A.; Ticha, H. *J. Non-Cryst. Solids* **1983**, *59,60*, 1015.
(25) Averyanov, V. L.; Gelmoni, B. L.; Kolmiets, B. T.; Lyubin, V. M.; Prikhodko, O. Yu.; Tsendin, K. D. *J. Non-Cryst. Solids* **1984**, *64*, 279.
(26) Tichy, L.; Ticha, H.; Benes, L.; Malek, J. *J. Non-Cryst. Solids* **1988**, *116*, 206.
(27) Tichy, L.; Ticha, H.; Triska, A.; Nagels, P. *Solid State. Commun.* **1985**, *53*, 399.
(28) Bhatia, K. L.; Parthasarathy, G.; Sharma, A.; Gopal, E. S. R. *Phys. Rev. B* **1988**, 38, 342.
(29) Elliott, S. R.; Steel, A. T. *Phys. Rev. Lett.* **1986**, *57*, 1316.
(30) Tohge, N.; Kanda, K.; Minami, T.; Yogyo-Kyokai-Shi. *J. Ceram. Soc. Jpn.* **1986**, *94*, 226.
(31) Rowland, S. C.; Ritland, F.; Haferburns, D.; Bienenstock, A. In *Proceedings of the 7th International Conference on Amorphous and Liquid Semiconductors*; Spear, W. E., Ed., Institute of Physics: Bristol, 1977; p 135.
(32) Shukla, R. K.; Swarup, S.; Agnihotri, A. K.; Nigam, A. N.; Kumar, A. *Philos. Magn. Lett.* **1991**, *64*, 165.
(33) Tohge, N.; Matsuo, H.; Minami, T. *J. Non-Cryst. Solids* **1987**, *95,-96*, 809.
(34) Baranovskil, S. D.; Bordovskil, G. A.; Kazakova, L. P.; Lebedev, E. A.; Lyubin, V. M.; Savinova, N. A. *Sov. Phys. Semicond.* **1984**, *18*, 633.
(35) Bordovsky, G. A.; Kazakova, L. P.; Lebedev, E. A.; Lyubin, V. M.; Savinova, N. A. *J. Non-Cryst. Solids* **1984**, *63*, 415.
(36) Kolomiets, B. T.; Lyubin, V. M. *Phys. Status Solidi* A **1973**, *17*, 11.
(37) Rabinal, M. K.; Ramesh Rao, N.; Sangunni, K. S.; Gopal, E. S. R. *Philos. Magn. B* **1994**, *70*, 89.
(38) Bhatia, K. L.; Malik, S. K.; Kishore, N.; Singh, S. P. *Philos. Magn. B* **1992**, *66*, 587.
(39) Malik, S. K.; Bhatia, K. L.; Kishore, N.; Phor, J. S. *J. Non-Cryst. Solids* **1992**, *142*, 55.
(40) Rahman, S.; Ramanan, M. V.; Sastry, G. S. *Phys. Chem. Glasses* **1992** *33*, 209.
(41) Rao, K. J. *Rev. Solid State Sci.* **1987**, *1*, 55.
(42) Vaidhyanathan, B.; Asokan, S.; Rao, K. J. *Pramana* **1994**, *43*, 189.
(43) Angell, C. A. *J. Phys. Chem. Solids* **1988**, *49*, 863.
(44) Borisova, Z. U. *Glassy Semiconductors*; Plenum Press: New York, 1981.
(45) Prasad, M. V. N. Ph.D. Thesis, Indian Institute of Science, 1987.
(46) Mohan. R.; Rao, K. J. *Mater. Res. Bull.* **1983**, *18*, 195.
(47) Tohge, N.; Minami, T.; Yamamoto, Y.; Tanaka, M. *J. Appl. Phys.* **1980**, *51*, 1048.
(48) Bhatia, K. L.; Malik, S. K. *Phys. Status Solidi B* **1991**, *168*, K51.
(49) Tronc, P.; Bensoussan, M.; Brenac, A.; Sebenne, C. *Phys. Rev. B* **1973**, *8*, 5947.
(50) Bridenbaugh, P. M.; Espinosa, G. P.; Griggiths, J. E.; Phillips, J. C.; Remeika, J. P. *Phys. Rev. B* **1979**, *20*, 4140.
(51) Polk, D. E.; Boudreaux, D. S. *Phys. Rev. Lett.* **1973**, *31*, 92.
(52) Rao, K. J.; Mohan, R. *Solid State Commun.* **1981**, *39*, 1065.
(53) Ribes, M.; Olivier-Fourcade, J.; Philippot, E.; Maurin, M. *Acta Crystallogr., Sect. B Fundam. Crystallogr.* **1974**, *30*, 1391.
(54) Rao, K. J.; Wong, J. *J. Chem. Phys.* **1984**, *81*, 4832.